Supporting Information for

Growth mechanism and atomic structure of group-IIA compound-promoted CVD-synthesized monolayer transition metal dichalcogenides

Shouheng Li[1], Shanshan Wang*[1,2], Tao Xu[3], Hui Zhang[1], Yuxiang Tang[3], Song Liu[4], Tian Jiang[3], Shen Zhou[1], Haifeng Cheng[1]

[1] Science and Technology on Advanced Ceramic Fibers and Composites Laboratory, College of Aerospace Science and Engineering, National University of Defense Technology, Changsha 410073, P. R. China

[2] Center for Nanochemistry, Beijing Science and Engineering Center for Nanocarbons

Beijing National Laboratory for Molecular Sciences, College of Chemistry and Molecular Engineering, Peking University, Beijing 100871, P. R. China

[3] College of Advanced Interdisciplinary Studies, National University of Defense Technology, Changsha 410073, P. R. China

[4] Institute of Chemical Biology and Nanomedicine (ICBN), State Key Laboratory of Chemo/Biosensing and Chemometrics, College of Chemistry and Chemical Engineering, Hunan University, Changsha 410082, P. R. China
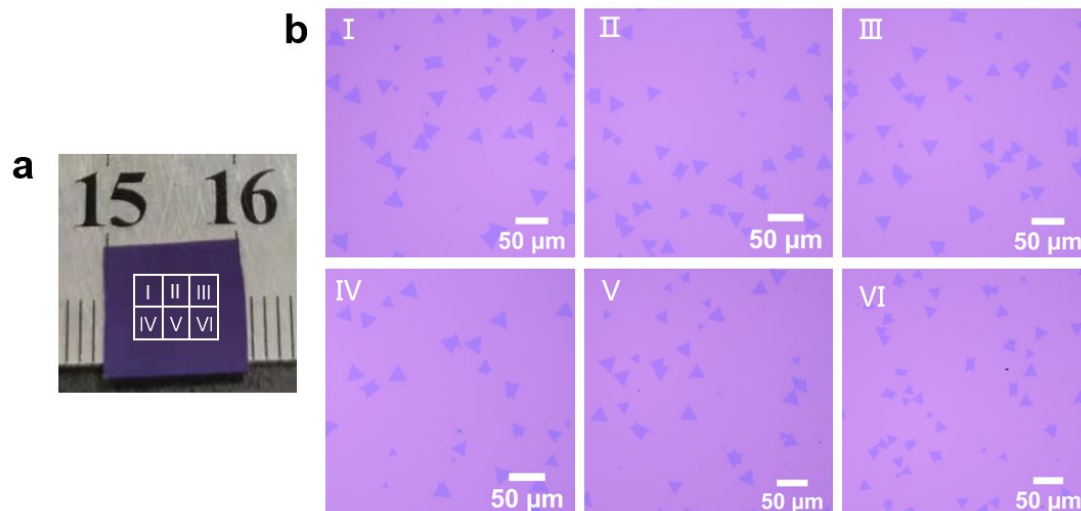
E-mail: wangshanshan08@nudt.edu.cn

Figure S1. Optical images of 2D MoS$_2$ grown on the six regions (section I to VI) of the SiO$_2$/Si substrate, respectively.

The width and length of the substrate loaded in the 1-inch quartz tube are both 1 cm. The CVD-grown 2D TMDs exhibit good homogeneity at the central region of the substrate, which is larger than 0.6cm×0.5cm. The growth results close to the substrate boundary are different from the central region, since the key growth conditions, such as the flow rate of the carrier gas, precursor concentration and the amount of the promoter adsorbed on the substrate at the boundaries are distinctive from the central area. As shown in Fig. S1a, we divided the central region of the substrate into 6 sections and displayed the corresponding optical images of the as-grown MoS$_2$ assisted by CaCl$_2$. Fig. S1b shows that the domain size, shape, and contrast in different sections are homogeneous, indicating the growth uniformity of the product at different substrate regions.
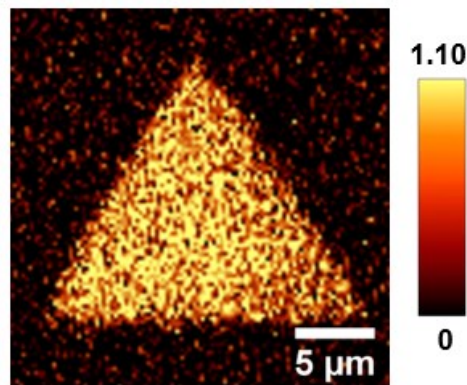
Figure S2. Raman map showing the spatial variation of the intensity ratio between the E_{2g}^1 and the A_{1g} Raman modes of an isolation MoS_2 domain. The intensity ratio is ~1.1 everywhere, indicating good spatial homogeneity of the MoS2 flake.
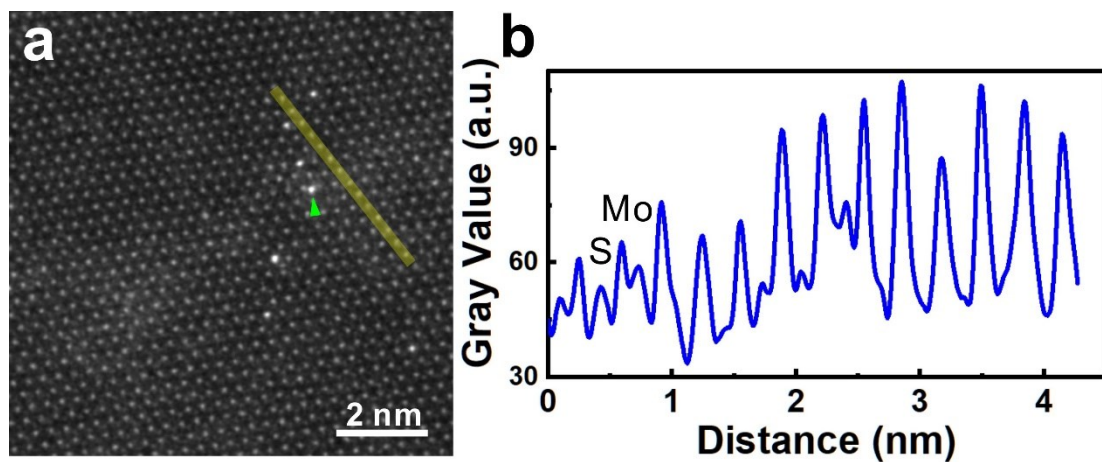

Figure S3. (a) ADF-STEM image of the Re doped MoS_2 monolayer. (b) Intensity line profile taken along the yellow line in panel (a). The increase of the background intensity indicates the presence of amorphous carbon on the sample surface.
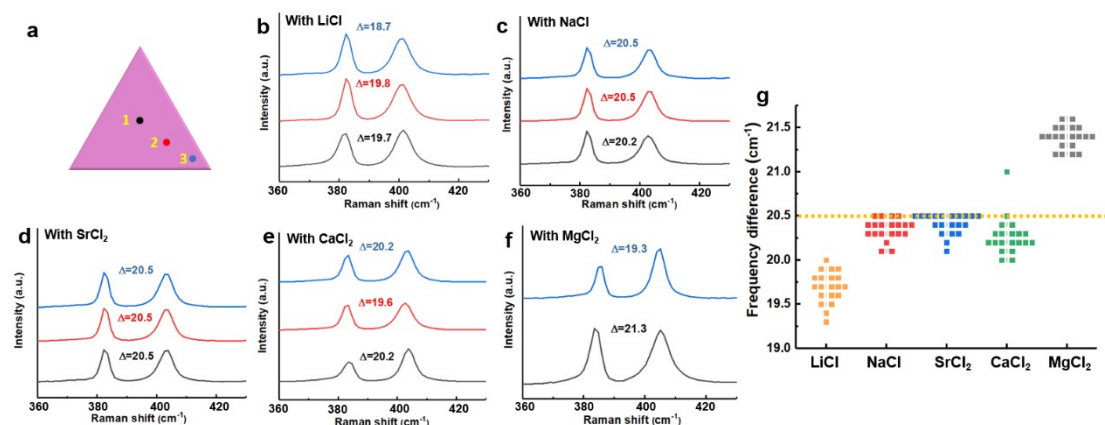
Figure S4. (a) Schematic illustration showing three representative locations from the center to the edge of the MoS_2 domain selected for the following collection of the Raman spectra. (b-f) Raman spectra taken from three different locations on MoS_2 domains grown with the promoters of LiCl, NaCl, $SrCl_2$, $CaCl_2$ and $MgCl_2$, respectively. The black, red, and blue curves correspond to the collection of Raman spectra from locations marked by 1, 2, and 3 in panel a. (g) Scattered plot showing the frequency difference between A_{1g} and E_{2g}^1 modes measured at the center of 20 domains randomly chosen on each substrate coated by different promoters.

A detailed Raman analysis was conducted to evaluate the thickness homogeneity of MoS2 grown with different promoters. Three representative spots locating from the domain center to the edge, respectively, were chosen for each MoS_2 flake to collect the Raman spectra in order to evaluate the thickness uniformity of the whole flake, as schematically illustrated in Fig. S4a. The frequency difference between the Raman modes of E_{2g}^1 and A_{1g} was extracted to determine the material thickness of the test area. As shown in Fig. S4b-f, when using LiCl, NaCl, $SrCl_2$ and $CaCl_2$ as promoters, the frequency difference between E_{2g}^1 and A_{1g} modes measured at different areas of the domain is small and the separation of the two peaks is lower than 20.5 cm^{-1}, indicating good thickness homogeneity and the monolayer thickness of the whole domain.[1] In contrast, when using $MgCl_2$ as the promoter, the frequency differences between the E_{2g}^1 and A_{1g} peaks collected at the domain center and on the edge are obvious, which are 21.5cm^{-1} and 19.3cm^{-1}, respectively. It suggests the

multilayer thickness at the domain center, which is consistent with the optical contrast in Fig. S5c. To access the homogeneity of the 2D flakes on the whole substrate, we randomly chose 20 domains on each substrate coated by different promoters and measured their Raman frequency difference at the domain center (Fig. S4g). Since 20.5 cm^{-1} is the frequency difference threshold for monolayer MoS$_2$, the points situating below the yellow dotted line of y= 20.5 indicate the single-layer thickness of the tested area. It can be seen that MoS$_2$ flakes grown assisted by LiCl, NaCl and SrCl$_2$ are all monolayer thickness at the domain center. For MoS$_2$ synthesized with the promoter of CaCl$_2$, there is only one data point locating above the dotted line, suggesting that only a small number of domains are few-layer thickness. For MoS$_2$ grown with the promoter of MgCl$_2$, almost all the data points are above the line, indicating the multilayer thickness at the MoS$_2$ domain center when using this type of the promoter. To sum up, the promoters of LiCl, NaCl, SrCl$_2$ and CaCl$_2$ can lead to monolayer MoS$_2$ with good thickness homogeneity. In contrast, even though MgCl$_2$ can also slightly facilitate the domain size expansion of MoS$_2$, the products exhibit multilayer thickness with poor uniformity.
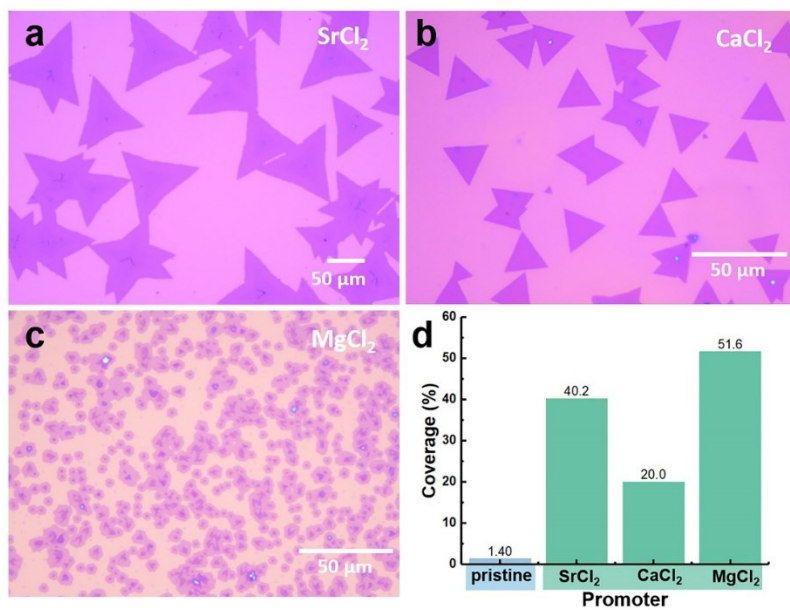
Figure S5. (a-c) Optical images of MoS_2 grown on the SiO_2/Si substrates spin-coated with alkaline earth metal salts including $SrCl_2$, $CaCl_2$ and $MgCl_2$. (d) Coverage of MoS_2 domains grown with and without alkaline earth metal salts, respectively.
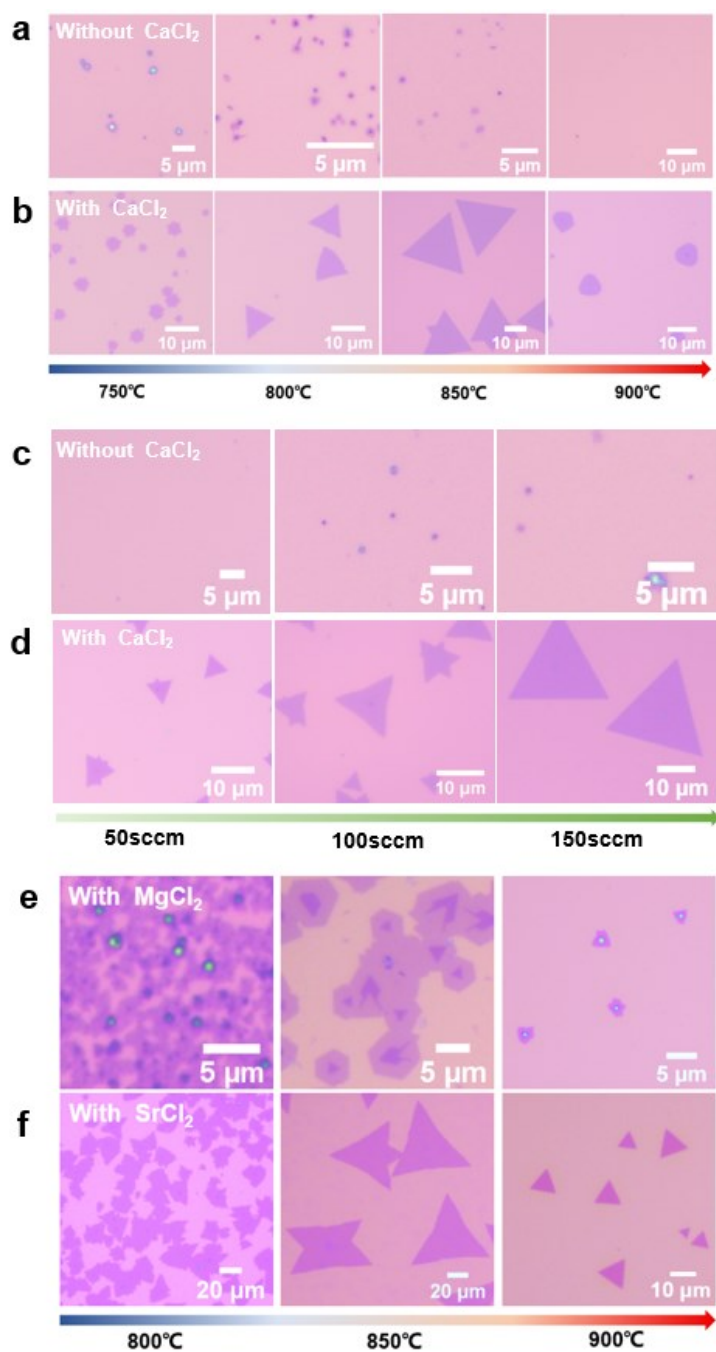
Figure S6. (a, b) Optical images of MoS$_2$ grown at 750 to 900°C without and with the promoter of CaCl$_2$, respectively. (c, d) Optical images of MoS$_2$ grown with Ar flow rates of 50, 100, and 150 sccm without and with using CaCl$_2$ as the promoter, respectively. (e, f) Optical images of MoS$_2$ grown at temperatures from 800 to 900°C using MgCl$_2$ and SrCl$_2$, respectively.

Fig. S6a and b are optical images of the MoS$_2$ growth at a series of temperatures from 750 to 900°C with and without the promoter of CaCl$_2$, respectively. It can be

seen that the addition of $CaCl_2$ leads to increased lateral size of MoS_2 at different temperatures between 750 and 900°C, confirming the universal effect of $CaCl_2$ in a broad range of temperatures. The domain size first increased as the growth temperature enhanced to 850°C and then shrank at 900°C. The enlargement of the domain size as a function of the growth temperature in the range of 750 and 850°C may be attributed to the increased mobility of the precursor on the substrate surface, thus leading to the formation of well-faceted, large triangular 2D crystals. When the temperature further raised to 900°C, the adsorption of precursor molecules on the surface may significantly decrease due to a relatively high substrate temperature, thus resulting in the reduction of the domain size. We also investigated the impact of the flow rate of the carrier gas (argon gas) on the growth results. Analogously, the promoting effect of $CaCl_2$ is verified in all the cases where the flow rates of Ar are 50, 100 and 150 sccm, respectively (Fig. S6c,d). The domain size of MoS_2 enhanced with the increased flow rate, which can be ascribed to the enhancement of the precursor feedstock to the targeted growth region. Finally, we studied the growth dependence on the substrate temperature using more types of promoters other than $CaCl_2$. Fig. S6e and f are optical images of the MoS_2 grown at a series of temperatures from 800 to 900°C using the promoters of $MgCl_2$ and $SrCl_2$, respectively. Compared with using no promoters in our system (the last three panel in Fig. S6a), both $MgCl_2$ and $SrCl_2$ exhibit promoting effect of increasing the lateral size of MoS_2 domains at a relatively broad temperature window.

To sum up, these results manifest versatility of the promoting effect of the group-IIB chlorides in a large synthesis window. The process parameters, such as the growth temperature and the flow rate, selected in the main text are optimal, which can both provide good MoS_2 quality and display pronounced difference between the products with and without the usage of the promoter.
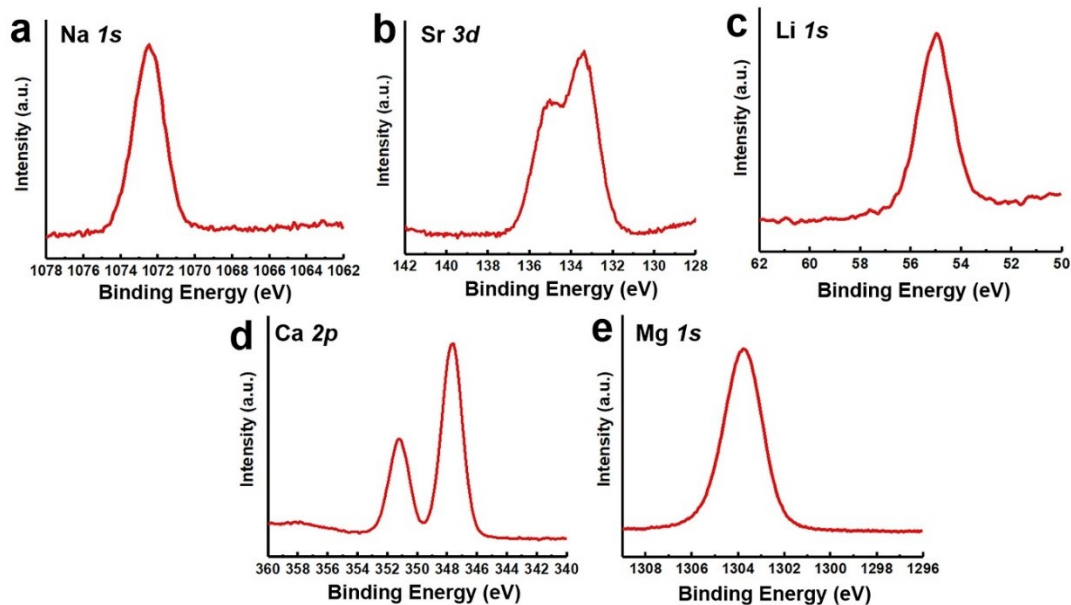
Figure S7. X-ray photoelectron spectroscopy (XPS) spectra showing the signals of metal elements on the MCl$_x$-modified SiO$_2$/Si substrates after annealing: Na 1s of NaCl-modified substrate (a), Sr 3d of SrCl$_2$-modified substrate (b), Li 1s of LiCl-modified substrate (c), Ca 2p of CaCl$_2$-modified substrate (d), and Mg 1s of MgCl$_2$-modified substrate (e).

Table S1. Chemical composition and corresponding calculated basicity of different MClx-modified substrates

Substrate	Atomic proportion of metal element [%]	Atomic proportion of Si [%]	Equivalent fractions of metal oxide X_{M_nO} [%]	Basicity of metal oxide $\Lambda[M_nO]$	Equivalent fractions of SiO₂ X_{SiO_2} [%]	Basicity of SiO₂ $\Lambda[SiO_2]$	Basicity of substrates Λ_{th}
SiO₂	0	26.85	0	/	100	0.48	0.48
Na@SiO₂	3.08	27.13	2.76	1.15	97.24	0.48	0.498
Sr@SiO₂	1.35	28.57	2.31	1.10	97.69	0.48	0.494
Li@SiO₂	2.67	26.79	2.44	1.00	97.56	0.48	0.493
Ca@SiO₂	1.10	28.80	1.87	1.00	98.13	0.48	0.490
Mg@SiO₂	1.14	28.26	1.98	0.78	98.02	0.48	0.486

For an M@SiO₂ substrate, its theoretical optical basicity can be calculated by the following steps: (1) split the substance of M@SiO₂ into two oxide components, MnO (M=Li, Na, Mg, Ca, and Sr, n=1,2) and SiO₂. MnO represents the alkali metal oxide or alkali metal earth oxide; (2) calculate the molar ratios between MnO and SiO₂ by elemental characterization; (3) figure out the "equivalent fractions" of MnO and SiO₂, denoted as X_{M_nO} and X_{SiO_2}, based on the molar ratios by taking the oxide states of the M and Si elements in the two oxides into account. The equivalent fractions represent the proportions of oxygen that the element M and Si contribute, respectively; (4) look up optical basicity values of MnO and SiO₂ from handbooks and calculate the theoretical optical basicity of the M@SiO2 substrate from the following formula:

$$\Lambda_{th} = X_{M_nO} \times \Lambda[M_nO] + X_{SiO_2} \times \Lambda[SiO_2]$$

The atomic proportions of Si and the metal elements were measured by XPS. The equivalent fractions of metal oxide (X_{M_nO}) and SiO$_2$ (X_{SiO_2}) can be expressed by the following formulas:

$$X_{M_nO} = \frac{ax}{ax + by}$$

$$X_{SiO_2} = \frac{by}{ax + by}$$

where a and b represent the oxidation states of the metal element and Si in metal oxide and SiO$_2$, respectively, and x and y are the atomic proportions of metal element and Si, respectively. Optical basicity of M$_n$O and SiO$_2$ are from the previous work.[2]
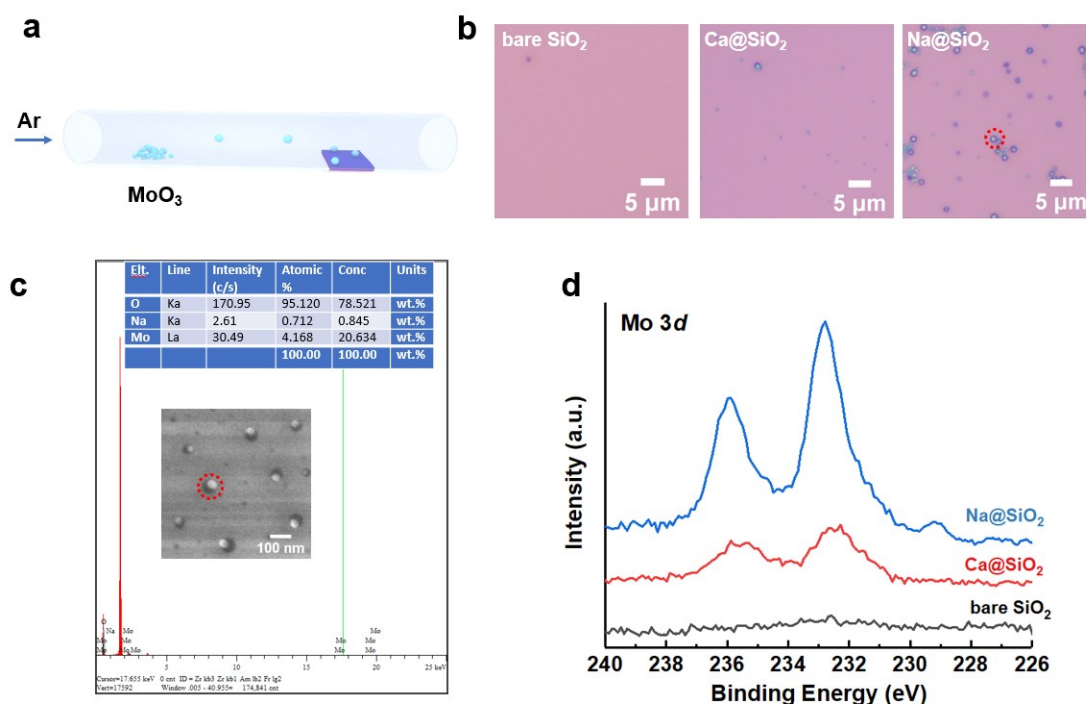
Figure S8. (a) Schematic illustration showing that only MoO$_3$ is placed in the tube and vaporized to deposit on substrates with different acidity/basicity. The XPS measurement will be conducted to characterize the adsorption amount of MoO$_3$ on different substrate. (b) Optical images showing different amounts of the precursor adsorbed on the Na@SiO$_2$, Ca@SiO$_2$ and the bare SiO$_2$ substrates, respectively. (c) EDX spectrum with the corresponding SEM image showing the measurement of the particle in the red dashed circle. (d) XPS spectra of Mo detected on the Na@SiO$_2$, Ca@SiO$_2$ and the bare SiO$_2$ substrates, respectively, after introducing vaporized MoO$_3$ into the system.

We conducted the CVD experiments without introducing sulfur, and then applied XPS characterization to measure the deposition amount of MoO$_3$ on different substrates with disparate acidity/basicity (Fig. S8a). It is noteworthy that the heating temperature of MoO$_3$ in this experiment was increased from 450°C in the original growth recipe to 600°C so that sufficient MoO$_3$ can be adsorbed on the substrate, thus facilitating the XPS detection. Na@SiO$_2$ (SiO$_2$ modified by NaCl), Ca@SiO$_2$ (SiO$_2$ modified by CaCl$_2$) and the bare SiO$_2$ were selected as typical substrates, which adopt decreased basicity. Fig. S8b shows the optical images of the adsorption result,

indicating that the ranking of the adsorption amounts on the substrate is bare $SiO_2<$ $Ca@SiO_2<$ $Na@SiO_2$, which is in line with the ranking of substrate basicity. Fig. S8c displays the EDX spectrum with the corresponding SEM image, confirming that the chemical constitution of the adsorbed particles on the substrate is molybdenum oxides. Fig. S8d shows the XPS spectra of Mo measured from the three substrates, respectively. The intensity of the Mo signal indicates decreased adsorption amount of the acidic MoO_3 as the basicity of the substrate decreases. The atomic contents of Mo on the $Na@SiO_2$, $Ca@SiO_2$ and bare SiO_2 substrates are 1.02%, 0.65% and 0.15%, respectively. These results well support our proposed acid-base match model in the manuscript, which attributes the promoting mechanism to an increase of the substrate basicity due to the usage of promoters, thus leading to sufficient adsorption of acidic precursor.
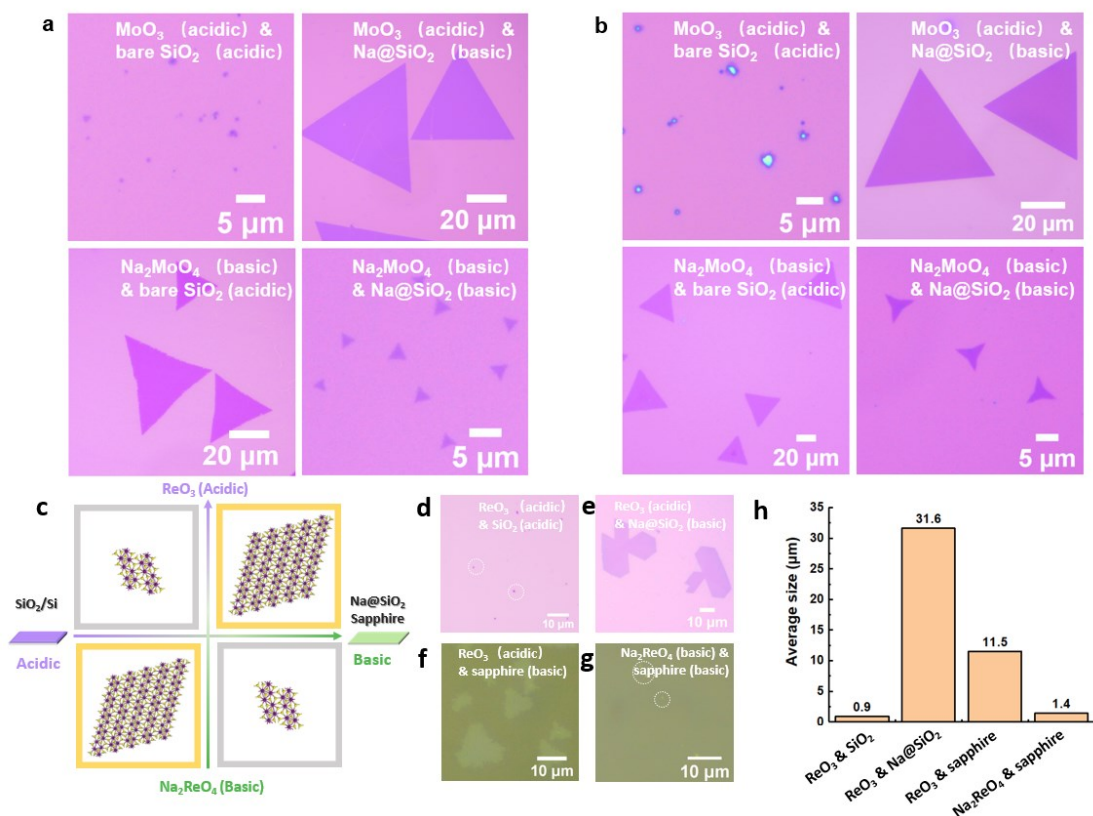
Figure S9. (a) Optical images showing the preparation results of 2D MoS_2 using four different combinations of precursors and substrates with the Ar flow rate of 50 sccm. (b) Optical images showing the preparation results of 2D MoS_2 grown at 800°C using four different combinations of precursors and substrates. (c) Four-quadrant diagram indicating the rational way to tailor the growth results of ReS_2 by designing the combination of precursors and substrates with different acidity/basicity. (d-g) Optical images showing the preparation results of 2D ReS_2 using four different combinations of precursors and substrates. (h) Histogram showing the average size of ReS_2 domains in Fig. S9d-g.

We have changed the flow rate and the growth temperature of the recipe and done similar comparison experiments as Fig. 7b-e in the main text to prove that the model suits the growth of MoS_2 under different conditions (Fig. S9a, b). Fig. R9c-h shows that this model also works for the growth of 2D ReS_2. The precursors we utilized include the acidic ReO_3 and the basic Na_2ReO_4, while the substrates include the acidic SiO_2, basic $Na@SiO_2$ (SiO_2 modified by NaCl to form basic sodium silicates)

and the basic sapphire.[2] They were divided into four groups for ReS_2 synthesis: acidic ReO_3 precursor with acidic SiO_2 substrate, acidic ReO_3 precursor with basic $Na@SiO_2$ substrate, basic Na_2ReO_4 precursor with basic sapphire substrate, and acidic ReO_3 precursor with basic sapphire substrate (Fig. S9c). It was found that the combination of basic substrate ($Na@SiO_2$ and sapphire) and acidic precursor (ReO_3) led to high quality two-dimensional products (Fig. R9e and f), while the growth results of the combination of acidic substrate with acidic precursor (Fig. S9d) and basic substrate with basic precursor (Fig. R9g) show the feature of inadequate precursor adsorption. Fig. S9h plots the average sizes of ReS_2 domains grown with these four different combinations the promoter and the substrate. The preparation result of ReS_2 is in line with our proposed model and expands the scope of use of the acid-base match mechanism.

REFERENCES

1   H. Li, Q. Zhang, C. C. R. Yap, B. K. Tay, T. H. T. Edwin, A. Olivier and D. Baillargeat, *Adv. Funct. Mater.,* 2012, **22**, 1385–1390.

2   J. A. Duffy, *J. Chem. Educ.* **1996**, *73*, 1138.